International Conference on Innovation and Engineering Technology (ICoIET) 2025
ISSN: XXX-XXX
Volume 1 Issue 01, 2025
https://icoiet.publikasi-untagcirebon.ac.id/

Performance of *Solar Still* Distillation with Paraffin In Tube As Thermal Energy Storage: Experiment and Numerical

Danang Dwi Prasetyo[1], Mustaqim[2], Rusnoto[3], Galuh Renggani Wilis[4], *Irfan Santosa[5]
[1,2,3,4,5] Department of Mechanical Engineering, Faculty of Engineering and Computer Science, Universitas Pancasakti Tegal, Indoneia

*Corresponding: irfansantosa@upstegal.ac.id

Abstract
This study aims to analyze the thermal performance and productivity of a single-slope solar still integrated with paraffin-in-tube thermal energy storage through experimental investigation and computational simulation. The research focuses on evaluating temperature distribution, evaporation–condensation behavior, and freshwater yield using paraffin as the thermal energy medium of the system. The results from both experimental and simulation approaches indicate similar thermal behavior with only slight temperature deviations. The CFD simulation tends to produce slightly higher temperature values due to ideal boundary conditions, whereas the experimental setup experiences natural heat losses through convection, conduction, and evaporation to the surroundings.

Keywords: Distillation, Single slope solar still, paraffin, thermal energy storage, CFD simulation

INTRODUCTION

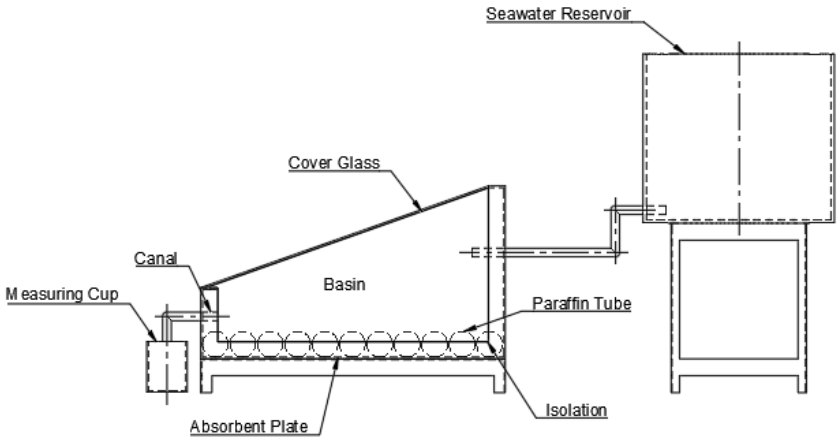
The increasing global demand for clean water remains one of the most pressing challenges in achieving sustainable development. This issue is particularly critical in arid and coastal regions where freshwater resources are scarce or inaccessible. As a response to this challenge, seawater desalination has emerged as a viable alternative for freshwater production. Among the various desalination techniques, solar still technology offers a sustainable and environmentally friendly solution by utilizing abundant solar energy to distill seawater into drinkable water (1). Despite its promise, conventional solar stills suffer from low productivity, primarily due to the intermittent nature of solar radiation and the absence of effective thermal energy retention. These limitations hinder their large-scale application and long-term viability. To address this, researchers have explored several enhancement strategies, including the integration of thermal energy storage (TES) systems. One of the most promising TES materials is phase change material (PCM), which can absorb, store, and release latent heat during phase transitions (2).

Paraffin wax, a commonly used PCM, has attracted considerable interest due to its high thermal capacity, chemical stability, low cost, and compatibility with solar desalination systems (3). When integrated into the basin or tubing of a solar still, paraffin wax helps maintain elevated water temperatures even after sunset, thereby extending the distillation process and increasing the overall yield of freshwater. Desalination in a solar still relies on fundamental heat transfer mechanisms: conduction, convection, and radiation. Solar energy heats the seawater, leading to evaporation, and the resulting water vapor condenses upon contact with a cooler surface, producing freshwater droplets (4,5). Radiation, in particular, plays a key role in transferring solar energy without a medium (6). However, due to the complexity of heat transfer interactions in solar stills, especially with the addition of PCM, experimental methods alone are often insufficient to fully understand system behavior.

To overcome these limitations, computational methods have become increasingly essential in thermal system analysis. Computational Fluid Dynamics (CFD) allows researchers to simulate heat transfer processes that are difficult or expensive to measure experimentally (7–9). While CFD has been widely applied in various industrial heat transfer problems (10). Application in the context of solar stills with integrated TES remains relatively underexplored. Computational simulation typically involves three key stages: preprocessing (geometry modeling, meshing, and boundary condition setup), solving (numerical computation using heat transfer equations), and postprocessing (result visualization through temperature contours, graphs, and performance metrics) (11,12). Therefore, this study aims to analyze the thermal and productivity performance of a single-slope solar still integrated with paraffin-in-tube thermal energy storage through both experimental investigation and computational simulation. The research focuses on evaluating temperature distribution, evaporation-condensation behavior, and freshwater yield under varying solar radiation intensities. The outcomes of this study are expected to contribute to the development of more efficient, low-cost, and sustainable solar desalination systems, particularly suited for deployment in rural and coastal communities.

RESEARCH METHOD

The research method used in this study is an experimental approach to construct a single-slope solar still distillation unit, as shown in Picture 1. The unit has dimensions of 90 cm in length, 60 cm in width, 51 cm in height at the rear, and 21 cm in height at the front, with a glass cover inclined at an angle of 30°. The phase change material (PCM), whose thermal properties are presented in Table 1, is paraffin encapsulated in cylindrical tubes with a diameter of 3 inches and a length of 50 cm, totaling 15 units, and used for thermal energy storage. The experimental setup was installed in East Tegal City, located at a latitude of –6.85174° and a longitude of 109.01498°. Temperature measurements include PCM temperature, seawater temperature, evaporation chamber temperature, glass cover temperature, ambient air temperature, and solar intensity, following the method used by Kumar and Maurya. (13).



Picture 1. Seawater distillation unit

Table 1. Thermophysical Properties Of Paraffin Wax (14)

No	Property	Value
1	The latent heat of melting	190 kJ/kg ℃
2	Liquid fraction point	55℃
3	Thermal transferability	0.19 W/m℃
4	Specific heat capacity	2.1 kJ/kg ℃
5	Heat capacity ratio	870 kg/m^3
6	Fluid density	791 kg/m^3

The parameters used in this study are based on the equations from (15).

1. Fourier's Law of Heat Conduction equation

$$\dot{Q}_{cond} = -k.A\frac{dT}{dx} \quad (1)$$

$\dot{Q}_{cond}$ = Rate of heat conduction (W)
k = Thermal conductivity (W/m·K)
A = Cross-sectional area (m^2)
dT = Differential of temperature (K or °C)
dx = Differential of distance (m)

2. Convection Heat Transfer equation

$$\dot{Q}_{conv} = hA_s\,(T_s - T_\infty) \quad (2)$$

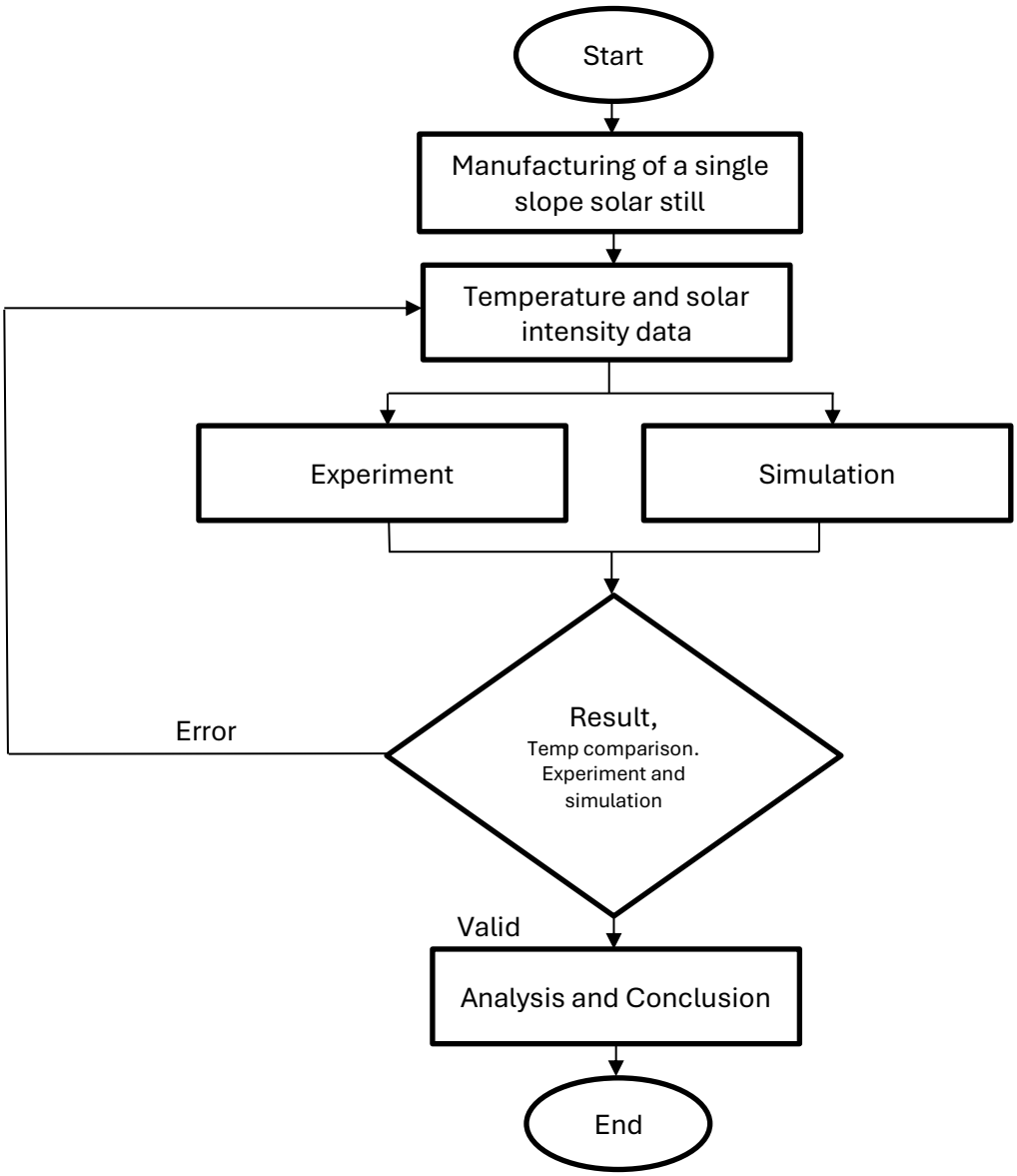
$\dot{Q}_{conv}$ = Convection heat transfer rate (W)
h = Convection heat transfer coefficient (W/m^2·K)
A_s = Surface area (m^2)
T_s = Surface temperature (K or °C)
T_∞ = Ambient fluid temperature (K or °C)

3. Radiation Heat Transfers equation

$$\dot{Q}_{emit,\ max} = \sigma A_s T_s^4 \quad (3)$$

$\dot{Q}_{emit,\ max}$ = Maximum rate of radiation emission (Blackbody) (W)
σ = Stefan-Boltzmann constant, where σ = 5.670 x 10^{-8} W/m^2·K^4 or 0.1714 x 10^{-8} Btu/h·ft^2·R^4
A_s = Surface area (m^2)
T_s = Absolute surface temperature (K).

A detailed research flow diagram was developed to illustrate the sequential stages of the experimental and simulation processes, as shown in Picture 2.

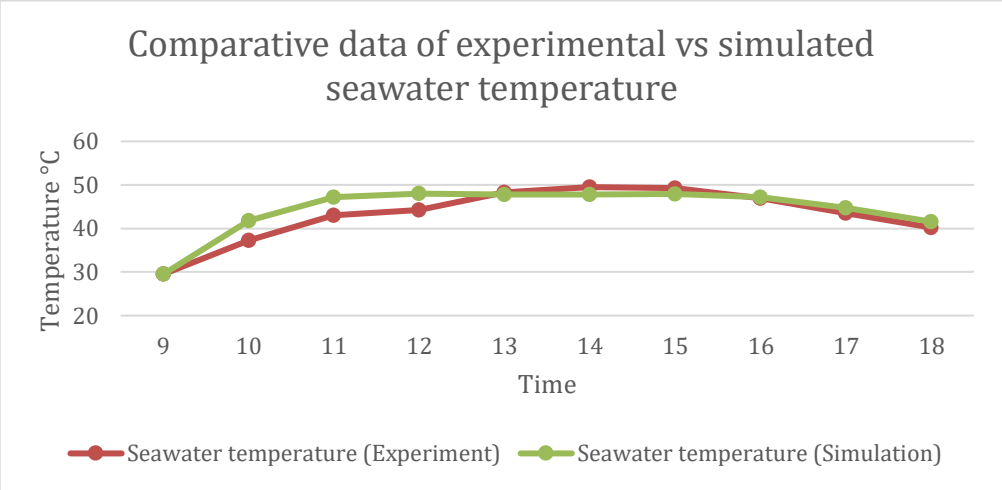


Picture 2. Flowchart Research

RESULTS AND DISCUSSION

Temperature data between experiment and simulation

The results of the experimental investigation were obtained from testing a single-slope solar still integrated with paraffin-based thermal energy storage, conducted from 9:00 a.m. to 6:00 p.m. The simulation study, involving geometry creation, boundary condition specification, mesh generation, and numerical setup, was performed using computational fluid dynamics (CFD) software. The temperature distributions obtained from both the experimental and simulation results are presented in Pictures 3, 4, and 5, respectively.

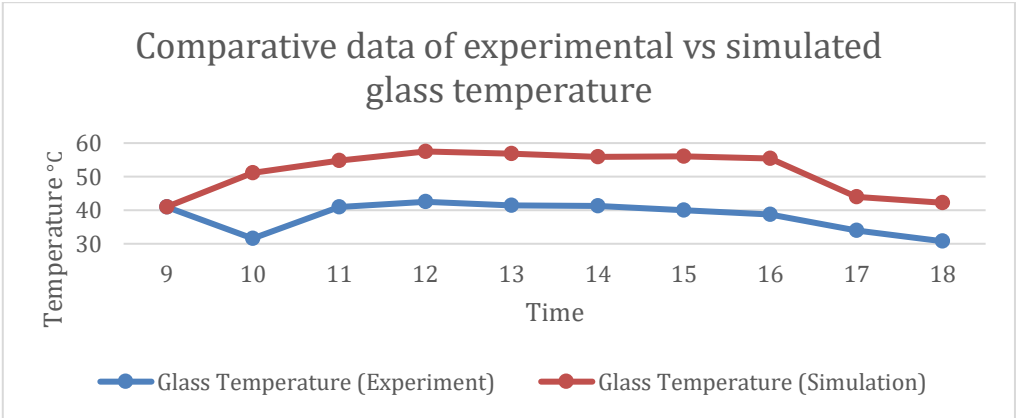


Picture 3. Comparison Of Seawater Temperatures Between Experiment And Simulation

The seawater temperature results obtained from both the experiment and simulation throughout the day are presented in Picture 3. Although both data sets exhibit a similar overall trend of increasing temperature from morning to early afternoon, followed by a gradual decrease towards evening, noticeable differences exist in the temperature values at various times.

In the morning hours (9:00 a.m.–11:00 a.m.), the simulation consistently predicts higher seawater temperatures compared to the experimental results. For example, at 10:00 a.m., the simulated temperature reaches 41.75°C, which is approximately 4.5°C higher than the experimental temperature of 37.25°C. This overestimation trend continues at 11:00 a.m. with a difference of 4.25°C. These deviations may be due to the idealized boundary conditions used in the simulation, such as assuming constant solar irradiance and neglecting heat losses caused by wind, evaporation, and conduction to the surroundings, which are present in the real experimental environment.

Between 12:00 p.m. and 3:00 p.m., the temperature difference narrows, and in some cases, the experimental temperatures slightly exceed those predicted by the simulation. At 1:00 p.m., the experimental temperature peaks at 48.25°C, slightly higher than the simulation's 47.85°C. This reversal could result from thermal inertia effects or localized environmental conditions not fully captured by the simulation model. From 4:00 p.m. to 6:00 p.m., both data sets show decreasing temperatures with differences within 1–1.5°C, indicating better alignment during the late afternoon period. Overall, the simulation model successfully captures the general thermal behavior and temperature profile of the seawater within the solar still, despite the discrepancies discussed.

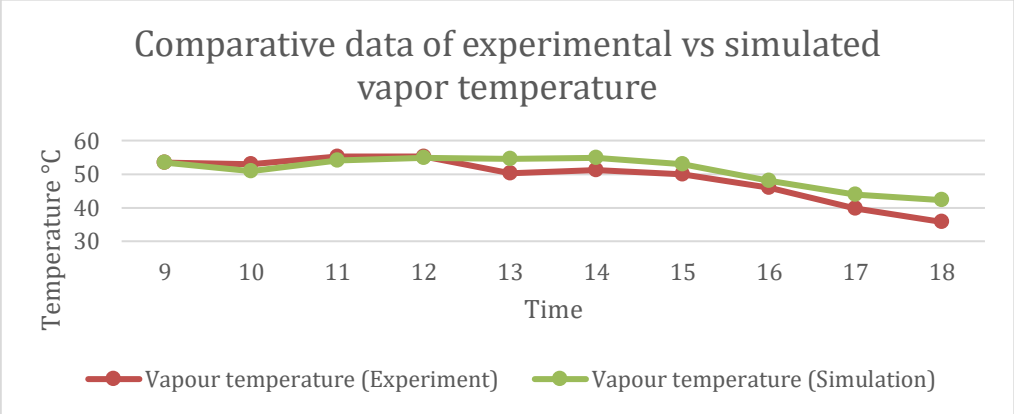


Picture 4. Comparison Of Glass Temperatures Between Experiment And Simulation

Picture 4 illustrates the glass cover temperatures measured experimentally and obtained from simulations at hourly intervals between 09:00 a.m and 18:00 a.m. The experimental glass temperatures ranged from 30.75°C to 42.50°C, while the simulated temperatures varied from 41°C to 57.50°C during the same period.

to 42.50°C, while the simulated temperatures varied from 41°C to 57.50°C during the same period. Specifically, the experimental temperature at 09:00 a.m was 41°C, decreased to 31.50°C at 10:00 a.m, and then gradually rose to a peak of 42.50°C at 12:00 p.m before declining towards the evening. In contrast, the simulation results showed a steady increase from 41°C at 09:00 a.m to a maximum of 57.50°C at 12:00 p.m, maintaining relatively high temperatures until late afternoon.

The significant temperature difference observed between experimental and simulated data is primarily attributed to the fresh water sprinkling performed every hour for five minutes during the experiment. This periodic sprinkling promotes enhanced condensation by cooling the glass surface, a process not replicated in the simulation model due to software limitations on incorporating intermittent cooling effects.



Picture 5. Comparison Of Vapor Temperatures Between Experiment And Simulation

Picture 5 illustrates the steam temperature obtained from both experimental measurements and simulation results at hourly intervals between 9:00 a.m and 6:00 p.m. Experimentally, the steam temperature started at 53.5°C at 9:00 a.m, exhibited a slight increase to 55.25°C at 11:00 a.m and 12:00 a.m, and then gradually decreased to 35.75°C by 6:00 p.m. The simulation data followed a similar trend, beginning at 53.5°C at 9:00 a.m, reaching a peak of approximately 54.85°C at 12:00 p.m and 2:00 p.m, before declining to 42.25°C at 6:00 p.m.

A comparison between experimental and simulation results reveals good agreement during the morning hours (9.00 a.m to 12.00 p.m), with temperature differences within 1.5°C. This is shown by the average percentage error value of less than 1% between the experiment and the simulation, as shown in Table 2.

However, from 1:00 p.m onwards, the simulation consistently overestimates the steam temperature compared to the experimental data, with discrepancies increasing up to 6.5°C by 6:00 p.m. These differences could be attributed to factors such as heat losses to the environment, unmodeled variations in steam flow, or simplifications within the simulation assumptions.

Table 2. Percentage Error

Time	Seawater (%)	Glass (%)	Vapor (%)
09.00	0	0	0
10.00	0.12080537	0.62380952	0.040566
11.00	0.09883721	0.33780488	0.022624
12.00	0.08474576	0.35294118	0.00724
13.00	0.008290155	0.36987952	0.08458
14.00	0.033333333	0.35393939	0.07024
15.00	0.026395939	0.4	0.06
16.00	0.00531915	0.4283871	0.04348
17.00	0.02873563	0.29411765	0.10314
18.00	0.0310559	0.37398374	0.18182

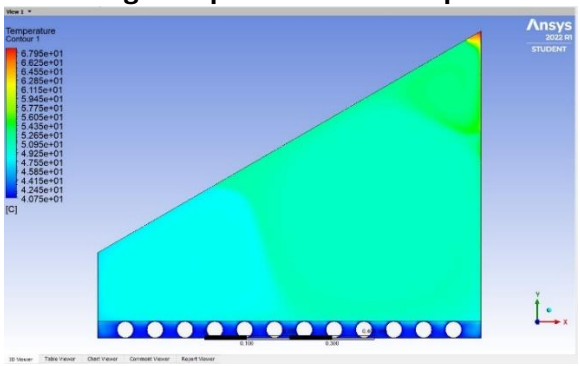
Based on the data presented in Table 2, the percentage errors in measurements of seawater, glass, and water vapor exhibited variation across different times of the day. At 9:00 a.m, all measured components showed no error, with a 0% error recorded for seawater, pipes, glass, and water vapor. At 10:00 a.m, the seawater measurement error rose to 0.12%, while errors for glass and water vapor were recorded at 0.62% and 0.04%, respectively. This trend indicates an initial increase in measurement deviation shortly after the start of observations.

Between 11:00 a.m and 1:00 p.m, the seawater error gradually decreased from 0.10% to 0.008%, while the glass error remained relatively stable, fluctuating slightly between 0.34% and 0.37%. Water vapor error varied slightly during this period, showing a low of 0.007% at 12:00 p.m and a rise to 0.08% at 1:00 p.m.

In the afternoon hours, from 2:00 p.m to 6:00 p.m, the seawater error remained low, ranging between 0.03% and 0.005%, indicating consistent measurement accuracy. Glass errors during this period fluctuated between 0.29% and 0.43%, while water vapor errors showed a gradual increase, peaking at 0.18% at 6:00 p.m.

Overall, the percentage errors observed were minor and stayed within acceptable tolerance levels for the instruments used. The variation in errors could be attributed to environmental factors such as temperature fluctuations, humidity, or instrument sensitivity throughout the day. These results suggest that the measurement system maintained a high degree of accuracy and reliability during the entire observation period.

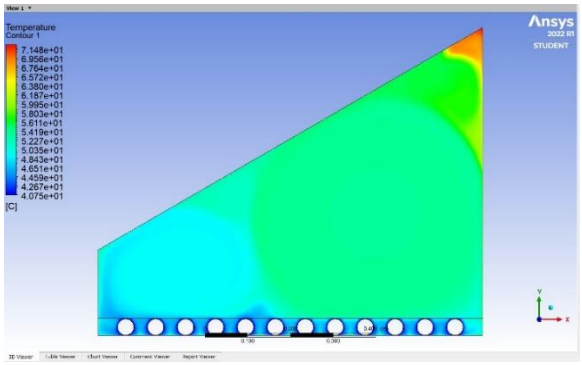
Temperature distribution of a single slope solar still with paraffin as heat storage energy



Picture 6. Temperature Distribution At 10:00 A.M

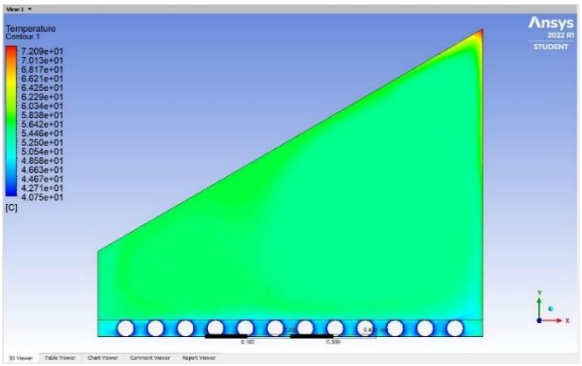
At 10:00 a.m., the temperature contour of the simulation results for the solar still model with a triangular geometry as shown in Picture 6. Based on the color scale on the left side, the temperature distribution ranges from 47.05°C to 67.95°C. It can be observed that the highest

temperature region, approximately 67–68°C, is located at the upper right corner near the inclined glass surface. This occurs due to heat accumulation at the upper section, which is influenced by the combined effects of solar radiation and natural convection that drives the warm air to move upward. The middle and upper left areas exhibit a temperature range between 55–60°C, represented by green to cyan colors, indicating a moderate temperature gradient and relatively uniform heat distribution in these zones. Meanwhile, the lower section near the water surface shows the lowest temperature, around 47–50°C, characterized by dark blue to light blue regions. This temperature reduction occurs because the water absorbs a portion of the heat, causing the air layer above it to remain cooler compared to the upper zone. This contour indicates a vertical temperature gradient, where heat transfer occurs predominantly through natural convection, causing warm air to rise and accumulate near the top surface, while cooler air remains near the bottom. This distribution pattern demonstrates that the upper region of the solar still tends to retain heat more effectively compared to the lower region, which is influenced by the presence of liquid water acting as a thermal sink.



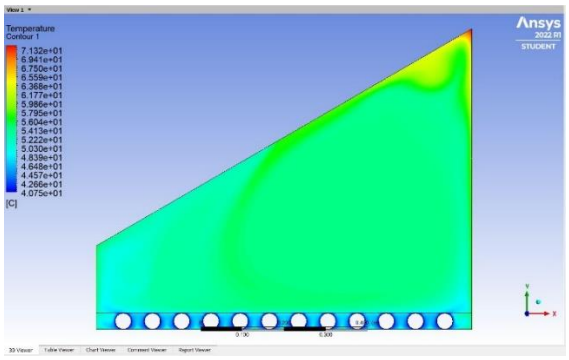
Picture 7. Temperature Distribution At 11:00 A.M

Picture 7 shows the temperature contour distribution of the solar still model at 11:00 a.m. The temperature in the system ranges from 40.75°C to 71.48°C, as indicated by the color scale on the left. The contour shows that the highest temperature zone, approximately 70–71°C, is located at the upper right corner of the glass cover. This indicates that heat accumulation occurs at the top region due to the combined effects of solar radiation and the upward movement of heated air caused by natural convection. The elevated temperature in this area suggests the maximum heat concentration point where vaporization is most likely to occur. The middle section exhibits moderate temperatures in the range of 55–65°C, represented by green to light blue colors. This indicates a relatively stable heat distribution in the air layer, showing that heat transfer within the chamber remains effective through convection. Meanwhile, the lower region near the water surface maintains the lowest temperature, between 40–50°C, which is illustrated in dark blue. This temperature difference occurs because the water absorbs part of the incoming heat energy for the evaporation process, resulting in a cooler boundary layer compared to the upper air region. The temperature gradient in this simulation demonstrates that thermal stratification occurs inside the chamber. The hot air accumulates near the inclined glass surface, while the cooler air remains near the bottom layer. This pattern indicates that heat transfer through natural convection is dominant, leading to a gradual increase in temperature at the upper region as solar radiation intensity increases towards midday.



Picture 8. Temperature Distribution At 12:00 P.M

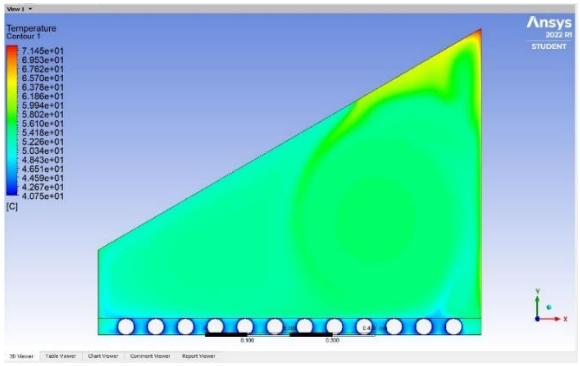
Picture 8 presents the temperature contour of the solar still simulation at 12:00 p.m. Based on the temperature scale shown on the left, the temperature distribution within the system ranges from 40.75°C to 72.09°C. The contour indicates that the highest temperature region, reaching approximately 72°C, is located at the upper right corner of the glass cover. This temperature rise occurs due to the peak solar radiation intensity around midday, causing significant heat accumulation near the glass surface. The upward movement of warm air through natural convection enhances the heat concentration in this region, which serves as the main zone for vapor condensation. The middle section shows a uniform greenish color corresponding to temperatures between 55–65°C, indicating that the air temperature inside the chamber has become more evenly distributed compared to earlier hours. This condition suggests that steady-state heat transfer begins to dominate the system, where the difference between upper and lower temperature gradients becomes relatively stable. In bottom region, particularly near the water surface, exhibits lower temperatures around 40–50°C, marked by blue color zones. This temperature difference is caused by continuous heat absorption by the water for the evaporation process, maintaining a relatively cooler boundary layer despite the overall increase in solar intensity. The contour at 12:00 p.m illustrates that the thermal energy within the chamber reaches its maximum value, indicating the highest heating phase during the simulation period. The pattern confirms that heat transfer is predominantly governed by natural convection and radiation, resulting in a concentrated temperature zone near the glass surface, which supports the evaporation–condensation cycle efficiency of the solar still system.



Picture 9. Temperature Distribution At 1:00 P.M

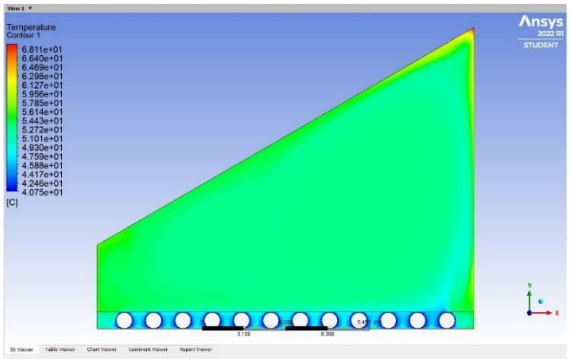
Picture 9 shows the temperature contour of the solar still simulation at 1:00 p.m. According to the temperature scale on the left, the temperature inside the chamber ranges from 40.75°C to 71.32°C. The highest temperature, approximately 71°C, is observed at the upper right corner of the inclined glass surface. This area experiences the greatest heat concentration due to continued solar radiation exposure and the accumulation of warm air driven upward by natural

convection. At this time, although solar intensity slightly decreases compared to noon, the system retains significant thermal energy due to the heat storage capacity of the materials and air inside the chamber. The middle region displays a relatively uniform green coloration corresponding to a temperature range of 55–65°C, indicating that the air within this section remains well mixed and thermally stable. This suggests that the convection process inside the solar still remains effective in distributing heat, maintaining the internal air temperature at a steady level. The bottom layer, particularly near the water surface, continues to exhibit the lowest temperature range, between 40–50°C, marked in blue. This occurs as the water continuously absorbs heat for evaporation, thus maintaining a relatively cooler interface compared to the air above it. The temperature distribution at 1:00 p.m shows a similar pattern to the previous hour but with a slightly reduced peak intensity. This indicates that the system has reached a thermal equilibrium state, where heat gain from solar radiation and heat loss through evaporation and convection are nearly balanced. The temperature gradient remains dominant from bottom to top, confirming that natural convection still plays a major role in the overall heat transfer mechanism within the solar still.



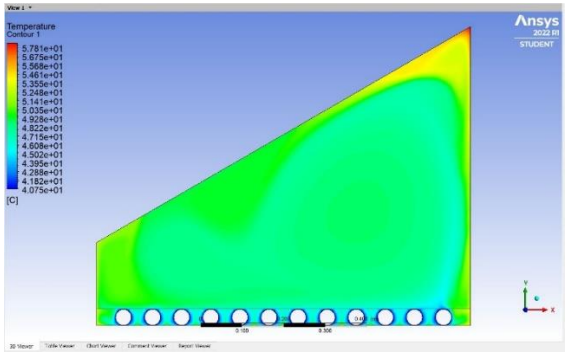
Picture 10. Temperature Distribution At 2:00 P.M

Picture 10 shows the temperature contour of the solar still simulation at 2:00 p.m. Based on the temperature scale displayed on the left, the internal temperature distribution ranges from 40.75°C to 71.45°C. The highest temperature, approximately 71°C, is located at the upper right region of the inclined glass surface. This area remains the main heat accumulation zone, where solar radiation continues to provide thermal energy, and warm air naturally rises through convective motion. Although solar intensity begins to decline slightly after midday, the stored heat within the air and material components maintains a high temperature near the top surface. The central region exhibits a wide greenish area corresponding to temperatures between 55–65°C, indicating that heat distribution inside the chamber remains relatively uniform. The steady color gradient suggests that natural convection circulation is still active, ensuring effective thermal mixing and preventing localized overheating. The lower section, particularly along the water surface, maintains a temperature range of 40–50°C, as indicated by the blue coloration. This consistent temperature pattern occurs due to ongoing heat absorption by the water layer for the evaporation process, resulting in a relatively cooler boundary region compared to the air above. The temperature contour at 2:00 p.m demonstrates that the system maintains thermal stability with a consistent temperature gradient from the bottom to the top of the chamber. The air temperature near the glass remains relatively high, ensuring continuous condensation potential, while the lower zone sustains the evaporation process. This pattern confirms that even after the peak solar radiation period, the system retains sufficient heat to support ongoing distillation performance.



Picture 11. Temperature Distribution At 3:00 P.M

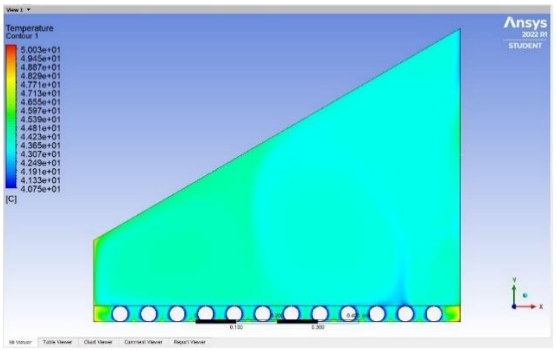
Picture 11 shows the temperature contours of the solar still model at 3:00 p.m. Based on the temperature scale shown on the left, the temperature inside the chamber ranged from 40.75°C to 68.11°C. The maximum temperature, around 68°C, was observed in the upper right corner of the inclined glass surface. This zone remains the area with the highest heat accumulation, although the temperature has decreased slightly compared to the previous hour. This decrease in maximum temperature is consistent with the decrease in solar radiation intensity in the afternoon. Nevertheless, the glass surface still retains significant heat due to continuous exposure to sunlight and residual thermal energy stored in the chamber. The central region shows a stable green color, corresponding to a temperature between 55–60°C, indicating that the air temperature in this area has become relatively uniform. This stability indicates that natural convection inside the solar still has reached a quasi-steady state, allowing for a balanced heat distribution between the upper and lower zones. Meanwhile, the lower portion, particularly along the water surface, maintains a lower temperature range of 40–50°C, represented by the blue color. This temperature difference continues to support the evaporation process, as heat from the upper zone transfers downward, thus maintaining the phase change mechanism between liquid water and vapor. Overall, the temperature contour at 3:00 p.m shows a gradual decrease in thermal energy, while maintaining the characteristic temperature gradient from bottom to top. The system remains thermally active, with a sufficient temperature difference between the evaporation and condensation zones to sustain the distillation process even in the afternoon.



Picture 12. Temperature Distribution At 4:00 P.M

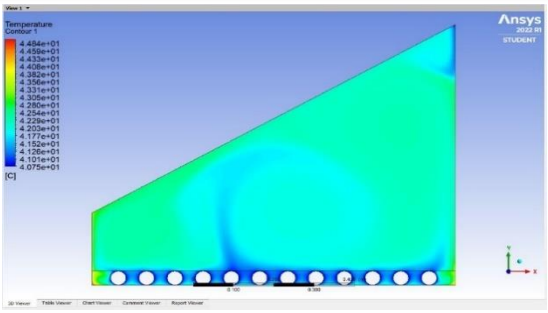
Picture 12 shows the temperature contour of the solar still simulation at 4:00 p.m. Based on the temperature scale on the left, the internal temperature of the system ranges from 40.75°C to 57.81°C, indicating a noticeable decrease compared to the previous observation times. The maximum temperature, approximately 57–58°C, appears at the upper right corner of the inclined glass surface. The temperature reduction in this region is associated with the declining solar radiation intensity in the late afternoon, which leads to lower heat input into the system. Although the heat accumulation zone remains at the top, its intensity diminishes as the ambient

temperature and incoming solar flux decrease. The middle section exhibits a dominant greenish color with temperatures between 50–55°C, showing that the overall heat within the chamber has begun to dissipate uniformly. This reflects a weakening of the natural convection circulation, as the temperature difference between the upper and lower layers becomes smaller. In the bottom layer, particularly along the water surface, a temperature range between 40–48°C is maintained, represented by the blue color. This consistent cooler zone indicates ongoing heat absorption by the water, although at a reduced rate due to the lower temperature gradient between air and liquid. This contour demonstrates that the system is entering a cooling phase, characterized by a gradual decrease in temperature throughout the chamber. The diminishing solar intensity reduces the thermal driving force for convection, resulting in a more uniform but lower temperature distribution. Despite this, the existing temperature difference between the bottom and top layers still supports limited evaporation and condensation processes within the solar still.



Picture 13. Temperature Distribution At 5:00 P.M

Picture 13 shows the temperature contour distribution of the solar still at 5:00 p.m. At this time, the solar radiation intensity has started to decrease, causing a gradual reduction in the overall temperature inside the basin. However, the paraffin wax used as a phase change material (PCM) still retains and releases the stored thermal energy, maintaining a relatively high temperature at the bottom surface. The temperature distribution indicates that the bottom region, where the PCM tubes are located, remains the warmest part with a maximum temperature of approximately 50.03°C. This residual heat from the PCM helps to sustain the evaporation process even during the late afternoon. Meanwhile, the upper region near the glass cover shows a lower temperature of around 41°C, caused by heat losses due to natural convection and radiation to the ambient air. The temperature gradient between the basin and the glass surface creates a continuous vapor condensation on the inner side of the glass, ensuring that the distillation process can still occur during this period. Localized thermal convection patterns can also be observed between the PCM tubes, represented by the slight variations in the contour colors, indicating air circulation driven by density differences between warm and cool air layers. The system at 5:00 p.m demonstrated effective thermal storage performance. The PCM successfully maintains a stable heat release, extending the operation of the solar still beyond peak sunlight hours, which contributes to higher overall distillate productivity.



Picture 14. Temperature Distribution At 6:00 P.M

Picture 14 shows the temperature contour distribution inside the solar still at 6:00 p.m. At this time, the solar radiation has significantly decreased as the sun is setting, resulting in a lower temperature throughout the system. The thermal energy source from direct solar input is minimal, and the temperature distribution indicates that the remaining heat within the system primarily originates from the stored energy inside the phase change material (PCM), paraffin wax. Temperature near the PCM tubes remains slightly higher, with a maximum temperature of around 44.84°C, while the upper region close to the glass cover has decreased to approximately 40°C. This shows that the PCM continues to release its latent heat, slowing down the cooling rate of the basin water. The released heat maintains a small temperature gradient between the basin surface and the glass cover, allowing the evaporation–condensation process to continue for a short period after sunset. The contour also reveals that the heat transfer has become more uniform compared to the previous hours, as the convection currents within the basin weaken due to reduced temperature differences. This condition marks the transition phase from active heating to passive cooling, where the PCM's thermal storage capability plays a crucial role in extending the operation time of the distillation process even under low solar intensity conditions.The system at 6:00 p.m demonstrates the effectiveness of PCM utilization in stabilizing the temperature and maintaining thermal performance after the absence of direct solar radiation, ensuring continuous freshwater production until the late evening.

CONCLUSION

From both experimental and simulation results, it can be concluded that the CFD model accurately represents the actual thermal performance of the solar still, with temperature deviations below 1%. Minor differences arise from idealized boundary conditions in the simulation and natural heat losses in the experiment. The thermal analysis indicates that higher solar intensity leads to higher temperatures of glass, vapor, and water, while lower intensity results in corresponding reductions. The integration of paraffin wax as a phase change material (PCM) effectively stabilizes the seawater temperature by storing excess heat during peak radiation and releasing it during low-radiation periods, thereby extending the distillation duration. Overall, the incorporation of PCM improves heat retention, minimizes temperature fluctuations, and enhances the efficiency and sustainability of solar desalination systems.

REFERENCES

1. Agrawal R, Singh KDP. Experimental investigation and computational modelling of double slope solar still integrated with eutectic phase change material. J Energy Storage [Internet]. 2022;52(PA):104802. Available from: https://doi.org/10.1016/j.est.2022.104802
2. Sonker VK, Sharma P, Ram R, Sarkar A. A CFD simulation analysis of the effects of PCM and nanoparticles stored in copper cylinders inside a solar still. J Energy Storage [Internet]. 2025;108(August 2024):115091. Available from: https://doi.org/10.1016/j.est.2024.115091
3. Thalib MM, Manokar AM, Essa FA, Vasimalai N, Sathyamurthy R, Garcia Marquez FP. Comparative Study of Tubular Solar Stills with Phase Change Material and Nano-Enhanced

Phase Change Material. Energies. 2020;13(15).
4. Bansal K, Kumar R, Krishna Mishra S, Kumar P, Sharma A. Validation and CFD modeling of solar still with nanoparticle coating on absorber plate. Mater Today Proc [Internet]. 2022;63:673–9. Available from: https://doi.org/10.1016/j.matpr.2022.04.744
5. Dsouza VL, Mallikappa DN. Performance analysis of step type solar still and comparison of the performance with evacuated tube collector coupled with single slope step type solar still. Mater Today Proc [Internet]. 2023;92:215–21. Available from: https://doi.org/10.1016/j.matpr.2023.04.347
6. Dhaoui S, Bouabidi A, Abdel-Aziz MM, Attia MEH. Performance enhancement of double slope solar still using cylindrical fins: Experimental and numerical analysis. Renew Energy [Internet]. 2024;237(PC):121825. Available from: https://doi.org/10.1016/j.renene.2024.121825
7. Loksupapaiboon K, Kamma P, Phromjan J, Phakdee S, Promtong M, Priyadumkol J, et al. Simulation-driven optimization of direct solar dryers for household use: A combined CFD and ANN-GA approach. Therm Sci Eng Prog [Internet]. 2025;67(July):104112. Available from: https://doi.org/10.1016/j.tsep.2025.104112
8. Dhaoui S, Souaissa K, Bouabidi A, Hadi Attia M El, Chrigui M. Numerical and experimental analysis of the effect of fin inclination angle on the performance of a double-slope solar still. Appl Therm Eng [Internet]. 2025;265(January):125659. Available from: https://doi.org/10.1016/j.applthermaleng.2025.125659
9. Mittal G. An unsteady CFD modelling of a single slope solar still. Mater Today Proc [Internet]. 2021;46:10991–5. Available from: https://doi.org/10.1016/j.matpr.2021.02.090
10. Pathak S, Jeyaraj T, Kumar P. A CFD and experimental analysis of a double-slope solar still with channel integration. Appl Therm Eng [Internet]. 2025;258(PB):124538. Available from: https://doi.org/10.1016/j.applthermaleng.2024.124538
11. Srishti, Paras, Kumar A. ANSYS Fluent-CFD analysis of a continuous single-slope single-basin type solar still. Green Technol Sustain [Internet]. 2024;2(3):100105. Available from: https://doi.org/10.1016/j.grets.2024.100105
12. Jeyaraj T, Kumar P, Pathak S. Enhancing double-slope solar still performance through integrated channel shape variations: An experimental and numerical simulation investigation. Renew Sustain Energy Rev [Internet]. 2025;209(March 2024):115106. Available from: https://doi.org/10.1016/j.rser.2024.115106
13. Kumar A, Maurya A. Experimental analysis and CFD modelling for pyramidal solar still. Mater Today Proc [Internet]. 2022;62:2173–8. Available from: https://doi.org/10.1016/j.matpr.2022.03.360
14. Hameed SA, Ali HHM, Fakhraldin SM. Augmenting the Thermal Efficiency of Solar Stills Using Phase Change Material on a Rotating Hollow Cylinder. Int J Heat Technol. 2025;43(3):1187–94.
15. Çengel, Yunus A. Ghajar AJ. HEAT AND MASS TRANSFER: FUNDAMENTALS & APPLICATIONS. Fifth Edit. New York: McGraw-Hill Education; 2015. 991 p.